Some Effects of a Seamount on Oceanic Flows

HSIEN WANG OU

Lamont-Doherty Geological Observatory of Columbia University, Palisades, New York

(Manuscript received 5 November 1990, in final form 22 May 1991)

ABSTRACT

To demonstrate some effects of a seamount on oceanic flows, we have considered a uniform, two-layer flow passing a right circular cylinder of arbitrary height in a rotating fluid. In the case of vanishing stratification, we first generalize previous results of low obstacles to an obstacle of finite height, and then show how the frictional regime provides a transition from partial to total blocking as the obstacle top approaches the surface.

In the case of general stratification, we have discerned various dynamical regimes according to blockage of the flows, characterized by distinctive interface signatures. For example, as the obstacle top rises through the water column, the axisymmetric doming of the interface first gives way to a reduced fore-and-aft symmetry when the lower layer is partially blocked, then becomes a net depression when the lower layer is totally blocked, and finally returns to its unperturbed level as both layers become totally blocked. We have derived the critical stratification below which there may be overlapping Taylor columns, and hence possible ventilation of the lower layer if surface cooling occurs. For typical oceanic conditions, this critical stratification corresponds to a baroclinic deformation radius measuring about one-half of the obstacle radius.

By generalizing the model results to a multiple-layer fluid, we have deduced mesoscale features similar to that observed over the Emperor Seamounts. When the model is applied to the Maude Rise in the Weddell Sea, it can explain the extensive ventilation of the water above the rise, with possible implications on the initiation and maintenance of the Weddell polynya.

1. Introduction

Because of the earth's rotation, which imparts some rigidity to a fluid column (Proudman 1916; Taylor 1917), even a submerged obstacle may effectively block an oceanic flow as if it extended to the surface. Ever since the presence of this peculiar fluid column was demonstrated by Taylor (1923) in the laboratory (hence called the "Taylor Column"), the subject has aroused intense theoretical interest, and many observed features in the planetary atmosphere and ocean have subsequently been interpreted as Taylor columns (Hide 1961; Hogg 1973; Owens and Hogg 1980; Gould et al. 1981). Most analytical models, however, have considered low obstacles immersed in a homogeneous or uniformly stratified fluid, which does not adequately describe most seamounts in an ocean containing a prominent thermocline. The desire to remove these limitations and broaden the model applicability prompts the present study.

2. The model

The model configuration is shown in Fig. 1. The ocean is approximated by a two-layer fluid, and the seamount is represented by a right circular cylinder. This latter approximation requires the flank of the seamount, where most of the depth variation occurs, to be narrow compared with the radius of the seamount. On the other hand, as is generally the case, the width of the flank is assumed to be much greater than the seamount height so that the topographic slope is everywhere much smaller than unity and the hydrostatic balance holds.

We further assume the unperturbed flow to be sufficiently broad that it is considered horizontally uniform, and the model domain sufficiently small that the Coriolis parameter f can be considered constant (taken to be positive to correspond to the Northern Hemisphere). In addition, the unperturbed flow is assumed to be vertically uniform so that the unperturbed interface is level. When combined with the hydrostatic balance, the flow then remains vertically uniform within each layer (i.e., outside a thin Ekman layer) despite their perturbation by the obstacle.

The object of the model is to determine the steady-state flow field and the associated interface relief as a function of the obstacle height, which may vary through the full depth range including the case when the obstacle protrudes above the surface. Although the model is highly idealized to facilitate the mathematics, it serves the purpose of elucidating some important physics, and we expect the deduced flow behavior to remain valid even in less idealized situations.

Corresponding author address: Dr. Hsien Wang Ou, Lamont Geological Observatory of Columbia University, Palisades, NY 10964.

© 1991 American Meteorological Society

Unauthenticated | Downloaded 01/15/25 03:25 PM UTC

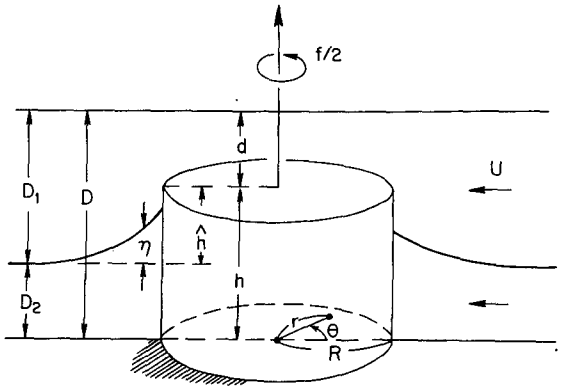

FIG. 1. A schematic of the model configuration in which a uniform two-layered flow passes a right circular cylinder of arbitrary height in a uniformly rotating fluid.

For the model derivations, all the variables have been nondimensionalized: the horizontal distance by the radius of the cylinder R, the water depth d (and the obstacle height h) by the maximum water depth D, the interface displacement η by the unperturbed interface depth D_1, and the horizontal velocity by the unperturbed flow speed U. For the terminology, the "inner" and "outer" regions designate the horizontal domains inside and outside the cylindrical boundary; the directions "left" and "right" refer to an observer facing downstream of the unperturbed flow; and a flow is said to be "partially" or "totally" blocked depending on whether the fluid from upstream occupies a portion or none of the inner region.

To facilitate discussions, we shall first consider the case of vanishing stratification before we discuss the case of general stratification.

3. Homogeneous fluid

Without stratification and hence current shear across the interface, one can integrate the continuity equation vertically through the water column (of depth d) to yield

$$\nabla \cdot \nu d = 0, \tag{3.1}$$

which allows the definition of a transport streamfunction ψ as

$$\nu = d^{-1}\mathbf{k} \times \nabla\psi. \tag{3.2}$$

Using a linear bottom drag, we consider the nondimensionalized vorticity equation

$$\nu \cdot \nabla q = -\alpha d^{-1}\mathbf{k} \cdot \nabla \times d^{-1}\nu, \tag{3.3}$$

where $q \equiv d^{-1}(1 + \epsilon\mathbf{k} \cdot \nabla \times \nu)$ is the potential vorticity scaled by f/D. The two dimensionless parameters are the Rossby number ϵ, defined as $U(fR)^{-1}$, and a friction parameter α, defined as $\alpha^*(fD)^{-1}$ with α^* being the resistance coefficient. To get a sense of their magnitude, let us take the typical case of $U \approx 20$ cm s^{-1}, $R \approx 100$ km, $f \approx 10^{-4}$ s^{-1}, $D \approx 5$ km, and $\alpha^* \approx 0.1$ cm s^{-1} (Csanady 1982) to yield $\epsilon \approx 2 \times 10^{-2}$ and $\alpha \approx 2 \times 10^{-3}$. While both parameters vary greatly in the ocean, based on this example, we shall only be concerned with the case $\alpha \ll \epsilon$. But despite the smallness of the frictional parameter, it is well known that the bottom drag singularly modifies the inviscid solution when closed streamlines are formed. Furthermore, as we shall see later, the inclusion of the bottom drag also avoids the singular transition when either layer becomes totally blocked.

On the other hand, we have neglected the horizontal diffusion in the vorticity equation, which is important within the shear layer around the obstacle. Indeed, we shall use this singular perturbation later to argue for a vanishing circulation when the flow is totally blocked. Another well-known singular behavior is the separation of the shear layer, which occurs in the laboratory when the Reynolds number reaches a magnitude of order 10 (Batchelor 1970; Takematsu and Kita 1978; Van Dyke 1982). In the ocean, one is less certain of the proper value of viscosity, but if one uses the often cited values of 10^6 to 10^8 cm s^{-1}, the Reynolds number corresponding to the above example lies in the range of 2 to 200. One thus cannot rule out the possibility of boundary-layer separation, which would considerably modify the flow derived below that assumes no separation.

If the water depth is everywhere much greater than α/ϵ, one may neglect the friction term in (3.3), which then states the conservation of potential vorticity. Since this potential vorticity has an upstream value of unity, it must retain such value everywhere in the model domain reached by the upstream flow. The fluid thus remains irrotational in the outer region, but the throughflow over the obstacle acquires an anticyclonic vorticity, the magnitude of which is proportional to the obstacle height. As this anticyclonic vorticity steers the flow to the left, the fluid eventually undergoes stagnation at the right edge of the cylinder when the obstacle is sufficiently tall. This critical height is 2ϵ, as derived by Ingersoll (1969), who has neglected the depth variation in (3.1) (i.e., the flow is essentially nondivergent or quasigeostrophic), and hence is valid only for infinitesimal ϵ. Johnson (1978), however, has not imposed such a limitation and obtained a critical height of $1 - (1 - 4\epsilon)^{1/2}$ for the onset of the stagnation. As plotted in Fig. 2, his value is greater than Ingersoll's and reduces to the latter only as ϵ approaches zero. Physically, the flow divergence associated with a finite depth change speeds up the irrotational component of the inner flow and hence counters the topographic steering and blocking of the flow. While the critical blockage height increases with Rossby number as expected—since one effectively mitigates the rotation effect—Johnson's solution shows additionally that as the Rossby number exceeds ¼, no blocking occurs regard-

Unauthenticated | Downloaded 01/15/25 03:25 PM UTC

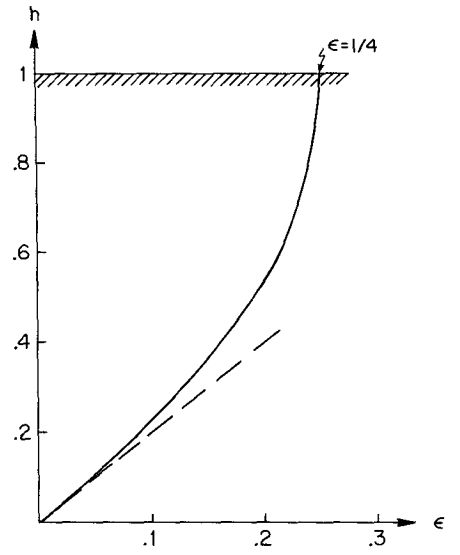

FIG. 2. The critical blocking height in a homogeneous fluid. The solid line is from Johnson (1978) and the dashed line is from Ingersoll (1969), who has assumed quasi geostrophy. The hatched area indicates the transition from partial to total blocking via a frictional regime.

less of the obstacle height. In midlatitudes, say, at 45° latitude, this Rossby number can be attained by a flow of 1 m s^{-1} passing an obstacle of 40 km radius.

As the obstacle height exceeds the critical value for onset of stagnation, closed streamlines are formed within which the fluid, being cut off from its ambient, no longer assumes the potential vorticity of the upstream flow, and indeed even a small bottom drag would eventually spin down the fluid and render it stagnant. This can be more formally shown by first combining (3.1) and (3.3) to yield

$$\nabla\cdot(\nu q d) = -\alpha\mathbf{k}\cdot\nabla\times d^{-1}\nu, \qquad (3.4)$$

and then integrating it over an area encircled by a closed streamline to show that the circulation and hence the flow vanishes along such a streamline. It follows then that the flow vanishes identically within a closed streamline, for otherwise there will be additional closed streamlines along which the flow does not vanish, contradicting the above deduction. This stagnant region has commonly been defined as the Taylor column; and the flow, as shown schematically in Fig. 3, is said to be partially blocked.

A solution satisfying this requirement of stagnation within a closed streamline has been constructed by Ingersoll (1969) for low obstacles, which shows a Taylor column anchored at the right edge of the cylinder and growing in size as the obstacle height increases. The analytical solution for a finite height obstacle has not been obtained, but the following argument illustrates that the Taylor column should remain tangent to the cylindrical boundary. One notes first that the Taylor column may not extend beyond the cylinder wall; otherwise, continuity of streamlines implies a negative vorticity along its boundary just outside the cylinder wall, contradicting the irrotationality of the outer flow. If, on the other hand, the Taylor column were to migrate inward and detach from the cylinder wall, the streamlines that connect the Taylor column to the far field would open at an angle that deviates finitely from the nominal right angle because of finite vorticity generated above the obstacle (appendix A). The solution thus may not vary continuously with the obstacle height, an obviously nonphysical situation. Together with the increasing blocking expected of a rising obstacle, one then expects the Taylor column to remain anchored at the right edge of the obstacle and its size to increase with the obstacle height, just as in the quasigeostrophic case.

Since the relative vorticity of the throughflow increases linearly with the obstacle height, its increasing expulsion to the left rim of the obstacle by an expanding Taylor column implies a circulation about the obstacle that increases less rapidly than the obstacle height. It nevertheless is finite as the obstacle top approaches the surface, which leads one to infer immediately that the above behavior may not remain valid in this asymptotic limit, since, as we shall argue next, when the obstacle protrudes above the surface (i.e., the seamount becomes an island), the circulation must vanish. To show this, we invoke the singular nature of the horizontal diffusion alluded to before which, although neglected in (3.3), facilitates a finite diffusive flux through the obstacle boundary because of its nonslip condition when the flow is totally blocked. So if the circulation just outside the diffusive boundary layer does not vanish, there would be a net diffusion of vorticity from the obstacle boundary (i.e., when integrated around the obstacle) that cannot be balanced by the inertial terms, which serve only to redistribute vorticity within this boundary layer. This argument obviously holds true even if the fluid has flexible surfaces as in a two-layer fluid. But for the particular case considered here with rigid surfaces, one can argue additionally through symmetry that the circulation must vanish. This is because without stretching or compression of the fluid column, the fluid cannot sense the rotation and hence may not favor either sense of the circulation that must then vanish.

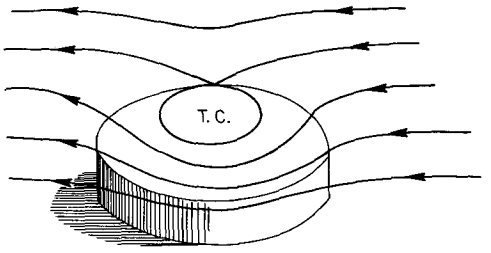

FIG. 3. A schematic of the barotropic flow partially blocked by a Taylor column.

Unauthenticated | Downloaded 01/15/25 03:25 PM UTC

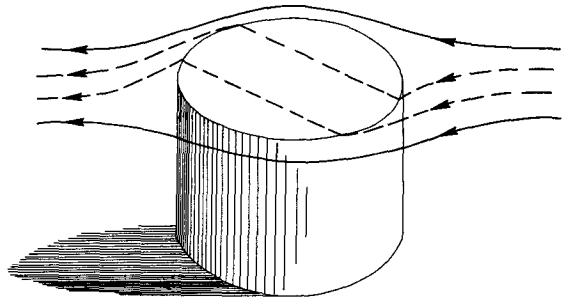

FIG. 4. A schematic of the barotropic flow in the frictional regime when the obstacle top extends to very near the surface. The dashed streamlines indicate the next order flows.

Independent of the above arguments, one also observes from (3.3) that bottom drag must become important over the obstacle as it approaches the surface (i.e., $d \ll \alpha/\epsilon$), in which case the inner flow has zero vorticity and hence zero circulation about the obstacle. Since a totally blocked irrotational flow is uniquely specified by its circulation about the obstacle (Batchelor 1970), the frictional regime thus provides a valid transition from partial to total blocking. The solution for the frictional regime is presented in appendix B and shown schematically in Fig. 4. To the lowest order, the outer flow is as a totally blocked flow that branches upstream of the obstacle, accelerating to a maximum speed of 2 at the midpoint along the cylindrical boundary before it decelerates toward the rear of the obstacle. The inner flow, being irrotational, is uniform. Its speed is vanishingly small (of order d), but it deflects finitely from the unperturbed flow by a clockwise angle of $\tan^{-1} d/\alpha$.

Because of the vanishing circulation about the obstacle when the flow is totally blocked, the perturbation velocity decreases at a more rapid rate of r^{-2} in the far field than when the flow is partially blocked (a rate of r^{-1} because of the finite circulation). It is the peculiarity of the earth's rotation that a submerged seamount perturbs the far field more than an island does. Furthermore, as we shall see later in the stratified case, only a submerged seamount can effectively disturb the interface and elicit a baroclinic response.

For the parameter constraint under consideration ($\alpha \ll \epsilon$), the transition from partial to total blocking via the frictional regime is rather abrupt and occurs only when the obstacle extends to very near the surface (i.e., $d \approx \mathrm{O}(\alpha/\epsilon) \ll 1$), as indicated schematically by the hatched area in Fig. 2. As we shall see later in the two-layer fluid, this nearly singular flow behavior, when applied to individual layers, would lead additionally to large interface excursion when either layer becomes totally blocked.

4. Stratified fluid

Since there may be velocity shear across an interface when the fluid is stratified, to formulate the frictional balance within closed streamlines one needs to incorporate an interfacial drag, which is assumed to depend linearly on the velocity difference across the interface. Furthermore, the resistance coefficient associated with the interfacial drag is assumed small compared with that of the bottom drag (Csanady 1982) so that the lower layer may be spun down by the bottom drag, even if it underlies a moving layer; whereas the upper layer may be stagnant only if it overlies a motionless lower layer. As a consequence, the Taylor column in the upper layer is wholly enclosed within the horizontal domain of the lower Taylor column, consistent with the expectation that the lower layer is more strongly blocked, or the presence of a Taylor cone when the fluid is continuously stratified (Hogg 1973).

With general stratification, one introduces two additional dimensionless parameters: namely, the unperturbed interface depth scaled by the maximum water depth ($\gamma \equiv D_1/D$) and the baroclinic deformation radius scaled by the obstacle radius ($r_C \equiv [g'D_e]^{1/2}[fR]^{-1}$, where g' is the reduced gravity and $D_e \equiv D_1 D_2/D$ is the effective depth). For a given Rossby number ϵ and interface depth γ, one can then examine the flow behavior as a function of the stratification r_C and the obstacle height h, as depicted in Fig. 5, where the horizontal dashed line indicates the unperturbed interface. Since different dynamical regimes, as seen below, are characterized by different flow blockages, the obstacle heights (h) that divide these

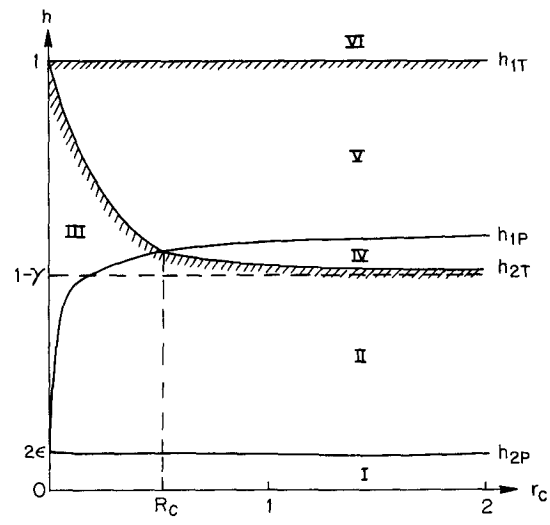

FIG. 5. Dynamical regimes (indicated by Roman numerals) on the parameter space of stratification (r_C) and obstacle height (h). The horizontal dashed line represents the unperturbed interface, the thick solid lines are blockage curves, and the hatched areas indicate the transition from partial to total blocking via frictional regimes. The figure is plotted to scale for $\gamma = 0.1$ and $\epsilon = 0.1$, with the upper-layer thickness magnified nine times to equal to that of the lower layer for easier display. The curves h_{2P}, h_{1T}, and the portions of the curves h_{1P} and h_{2T} that bound Regime IV are exact, while the remaining portions of the blockage curves are schematic.

Unauthenticated | Downloaded 01/15/25 03:25 PM UTC

regimes will be called blockage curves (the thick solid lines in Fig. 5). The appended subscripts 1 and 2 refer to the upper and lower layer, respectively, and the subscripts P and T indicate the obstacle height above which a "partial" and "total" blockage of the respective layer occurs. To limit the scope of the following discussions, only the case $\epsilon \ll 1$ will be considered, which, as seen earlier, generally applies in the ocean and represents the case of maximum topographic effect.

To draw crudely the blockage curves, one needs only to determine their end points and then join these points by smooth curves. In the limit of vanishing stratification, there is no distinction between the flows in the two layers; hence, there is only one set of critical heights for partial and total blockage, given by 2ϵ and 1, respectively. In the other extreme of strong stratification, the interface becomes rigid and remains unperturbed by the obstacle. The flows in the two layers are thus decoupled and respond independently to a protruding obstacle as predicted by the homogeneous model, resulting in the two sets of critical heights as plotted in Fig. 5. Connecting the end points, one observes that the parameter space is divided into six dynamical regimes (indicated by Roman numerals) characterized by the combined property of blockage of the two layers. Because the enhanced stratification has opposite effects on the flows in the two layers—it increasingly blocks the lower-layer flow while insulating the upper-layer flow—the blockage curves h_{1P} and h_{2T} have opposite slopes, resulting in their intersection at some critical stratification R_C. Depending on whether the stratification is weaker or stronger than this critical value, the flow undergoes different dynamical regimes as obstacle height increases, as discussed below.

a. *Regime I ($h < h_{2P}$)*

In this regime, neither layer is blocked. Since the obstacle is low ($h = O(\epsilon) \ll 1$), the flow is nondivergent and one can define streamfunctions as

$$\nu_{1,2} \equiv \mathbf{k} \times \nabla\psi_{1,2}, \tag{4.1}$$

which satisfy the nondimensionalized equations,

$$\nabla^2\psi_1 = -\epsilon^{-1}\eta, \tag{4.2}$$

$$\nabla^2\psi_2 = (1-\gamma)^{-1}\epsilon^{-1}(\gamma\eta - h), \tag{4.3}$$

$$\psi_1 - \psi_2 = -(1-\gamma)^{-1}r_C{}^2\epsilon^{-1}\eta. \tag{4.4}$$

The first two equations state the conservation of potential vorticity so that the relative vorticity is proportional to the change of layer thickness. The last equation is a combination of the geostrophic balance, which relates the streamfunctions to the pressure fields, and the hydrostatic balance, which relates the pressure difference of the two layers to the interface displacement.

Equations (4.2) through (4.4) can be combined to yield a single equation in η

$$\nabla^2\eta = r_C{}^{-2}(\eta - h), \tag{4.5}$$

which is subject to the boundary condition that

$$\eta \to 0 \quad \text{as} \quad r \to \infty, \tag{4.6}$$

since there is no vertical shear in the far field. One observes immediately from Eqs. (4.5) and (4.6) that for an axisymmetric obstacle $h = h(r)$, the interface relief has the same symmetry. Furthermore, it can be shown that η must be everywhere positive and bounded above by the maximum obstacle height, or

$$0 < \eta < h_{\max}. \tag{4.7}$$

This is because otherwise, the far-field condition (4.6) implies that η has a negative minimum or a positive maximum greater than $h_{\max}$, contradicting the sign of (4.5) at such extrema. Indeed, it is trivial to see that the lower bound is approached in the strongly stratified limit ($r_C \to \infty$) as (4.5) implies $\nabla^2\eta \to 0$ and hence $\eta \to 0$ because of (4.6). On the other hand, in the limit of weak stratification ($r_C \to 0$), (4.5) implies $\eta \to h$, or the interface relief simply mimics that of the underlying topography.

The solution to (4.5) and (4.6) is presented in appendix C, which is plotted on the left half of Fig. 6a for the case of $\gamma = 0.1$, $r_C = 1$, and $\epsilon^{-1}h = 1$. It is seen that the interface domes over the obstacle, the amplitude of which decays away from the obstacle with an e-folding distance given by the baroclinic deformation radius. This doming is a direct consequence of a lower layer that is more compressed (hence more anticyclonic) than the upper layer and may not be used to infer the presence of a Taylor column, as done in some observational studies. Rather, as we shall see below, it is the breaking of the axial symmetry that is indicative of a Taylor column.

To solve for the flows in the two layers, one can decompose them into barotropic (ψ_T) and baroclinic (ψ_C) components as

$$\psi_1 = \psi_T + (1-\gamma)\psi_C \tag{4.8}$$

$$\psi_2 = \psi_T - \gamma\psi_C, \tag{4.9}$$

which satisfy the uncoupled equations,

$$\nabla^2\psi_T = -\epsilon^{-1}h \tag{4.10}$$

and

$$\psi_C = -(1-\gamma)^{-1}r_C{}^2\epsilon^{-1}\eta. \tag{4.11}$$

The barotropic component thus corresponds to the flow in a homogeneous fluid as derived by Ingersoll (1969), and the baroclinic component is proportional to the interface displacement as given in appendix C. Accordingly, stratification affects the flow significantly only within a baroclinic deformation radius from the obstacle, outside of which the flow behaves as if the fluid is homogeneous. The flows of the two layers are plotted on the right half of Fig. 6a (solid lines for the

Unauthenticated | Downloaded 01/15/25 03:25 PM UTC

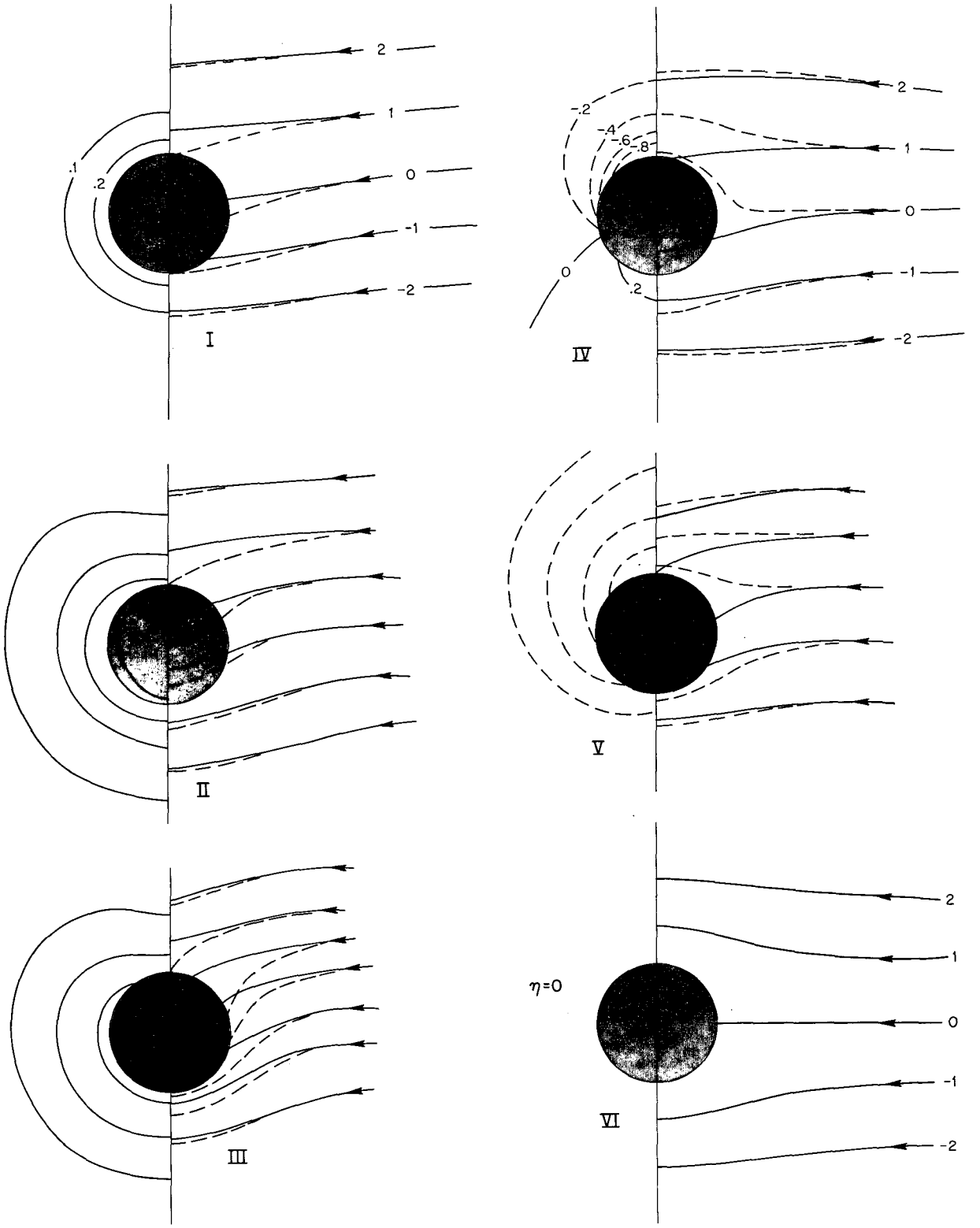

FIG. 6a–f. The flow fields and the interface relief for various dynamical regimes. Since both fields are fore-and-aft symmetric, they are plotted on adjoining half-planes. The streamlines (solid lines for the upper and dashed lines for the lower layer) are plotted on the right-half panel, and the contours of the interface displacement ($\epsilon^{-1}\eta$, solid for positive and dashed for negative values) on the left-half panel. Figures 6a, 6d, and 6f are exact while the others are schematic. The parameter values for Figs. 6a and 6d are $\gamma = 0.1$, $r_C = 1$, and either $\epsilon^{-1}h = 1$ (a) or $\epsilon^{-1}\hat{h} = 1$ (d).

Unauthenticated | Downloaded 01/15/25 03:25 PM UTC

upper and dashed lines for the lower layer), which shows greater deflection of the lower-layer flow. Because of the doming of the interface, the outer flow has cyclonic (anticyclonic) vorticity in the lower (upper) layer, which reduces (increases) the anticyclonic circulation along the obstacle boundary to the common negative value in the far field where baroclinicity vanishes.

As the obstacle height increases (see appendix C), a stagnation point is first formed in the lower layer at the right edge of the obstacle; the critical blockage height (h_{2P}) has been plotted in Fig. 5, which, as expected, decreases with stratification.

b. Regime II ($h_{2P} < h < h_{1P}, h_{2T}$)

In this regime, a closed streamline is formed in the lower layer within which the lower layer is stagnant, being spun down by a bottom drag against a negligible interfacial drag from above. Due to the coupling of the two layers through interface displacement, analytical solutions may not be obtained in this regime. But following similar arguments put forth for the homogeneous fluid, one deduces a similar behavior of the Taylor column in the lower layer; namely, that it is anchored at the right edge of the obstacle where there is abrupt change of the layer thickness and that it grows in size with the obstacle height. One modification of the earlier argument is that the outer flow is no longer irrotational but has cyclonic vorticity in the lower layer due to the uplift of the interface—which more strongly prevents the encroachment of the Taylor column into the outer region.

Within the Taylor column, (4.4) implies that the isobaths of the interface relief align with the upper-layer flow (i.e., reduced gravity), which are thus no longer axisymmetric, but assume the reduced fore-and-aft symmetry of the flow field. Since regardless of the detailed coupling of the upper-layer flow to the interface displacement, the upper-layer flow is anticyclonic due to general doming of the interface. The alignment of the two fields within the horizontal confine of the lower Taylor column results in the convoluted interface relief, as shown schematically in Fig. 6b. As alluded to before, it is thus the breaking of the axisymmetry of the interface relief that signals the presence of a Taylor column. The flows in the two layers are also plotted in Fig. 6b, which shows a partially blocked lower layer.

c. Regime III ($r_C < R_C, h_{1P} < h < h_{2T}$)

In this regime, there is also a Taylor column in the upper layer that, as remarked earlier, is wholly enclosed within that of the lower layer. Within the common domain of stagnation, (4.4) implies a level interface, resulting in an interface relief as plotted schematically in Fig. 6c. When compared with Regime II (Fig. 6b), the interface relief thus exhibits the additional feature of a level terrace punctuating the right flank of the dome. As plotted in Fig. 6c, the flows in both layers are partially blocked.

Just as a small bottom drag may spin down the fluid within a closed streamline, a stagnant fluid, being cut off from the ambient, is more susceptible to alteration by diabatic fluxes. In particular, in this regime of overlapping Taylor columns, even a small surface cooling may eventually break down the stratification and ventilate the lower layer. Although it is beyond the scope of the present model to incorporate diabatic processes, one expects the thermal configuration as depicted in Fig. 6c to be significantly modified when there is surface cooling, with a weakened stratification and possible homogenization of a whole fluid column above the obstacle.

d. Regime IV ($R_C < r_C, h_{2T} < h < h_{1P}$)

For stratification greater than the critical value R_C, one proceeds from Regime II to Regime IV with increasing obstacle height, in which the lower layer is totally blocked while the upper layer is not blocked. The value of R_C thus marks the critical stratification above which the lower layer is always insulated from the air–sea fluxes by a moving upper layer regardless of the obstacle height. To determine the value of R_C, one notes that in this regime, both layers have experienced only a small fractional change of the layer thickness and hence quasigeostrophy applies. The governing equations are thus given by (4.2) through (4.4) in the outer region and an equation similar to (4.2) in the inner region, with η replaced by the obstacle height above the unperturbed interface $\hat{h}$ $\{\equiv\gamma[h-(1-\gamma)]$, which has been scaled as $\eta\}$. The boundary conditions at $r = 1$ are that the upper-layer flow be continuous and the lower-layer flow has a zero circulation. This latter condition is a consequence of the total blocking of the lower layer, as discussed in section 3. The analytical solution, presented in appendix D, allows the derivation of the blockage heights h_{1P} and h_{2T}, as well as the critical stratification R_C where the two intersect. In Fig. 7, R_C is plotted as a function of the unperturbed interface depth γ. As expected from Fig. 5, R_C increases with decreasing γ, with a value of zero when $\gamma = 1$ and approaches 0.54 as γ approaches zero. Since in the ocean γ is generally small (i.e., thermocline is shallow relative to the ocean depth), the critical stratification R_C then corresponds to a baroclinic deformation radius measuring about half the obstacle radius, which serves as a useful criterion for possible ventilation of the Taylor column in the lower layer.

The interface relief in this regime is plotted in Fig. 6d, which is seen to differ qualitatively from the previous cases. While it may still be elevated to the left of the obstacle, it dips ostensibly downward at the right flank of the obstacle. Indeed, as shown next, there is a net downward displacement of the interface when in-

Unauthenticated | Downloaded 01/15/25 03:25 PM UTC

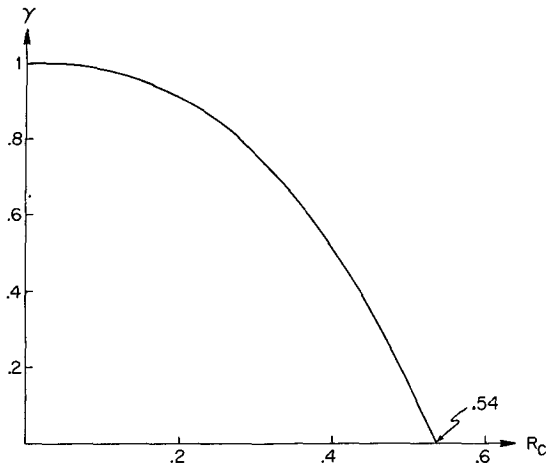

FIG. 7. The critical stratification R_C as a function of the unperturbed interface depth γ.

tegrated over the outer region. Since in the outer region (4.2) through (4.4) apply, the barotropic flow as defined in (4.8) and (4.9) is irrotational and hence has uniform circulation. This circulation, being the weighted mean of its values in the two layers, is bounded by these values, which is also the common value both layers tend to in the far field. Since along the obstacle boundary, the upper-layer circulation is more anticyclonic than that of the lower layer (being zero because of total blocking), the upper (lower) layer must gain (lose) vorticity in the outer region; hence, the net interface displacement is downward. Comparing Fig. 6d with Fig. 6c, one observes that it is the emergence of a strong lower-layer flow along the right flank of the obstacle that causes this precipitous dipping of the interface there. While the solution in this regime shows that the interface remains elevated to the left of the obstacle, one expects it to become depressed everywhere when the obstacle is sufficiently tall (i.e., the circulation in the upper layer is sufficiently large).

As in the homogeneous fluid, this transition from partial to total blocking of the lower layer occurs rather abruptly via a frictional regime when the layer thickness above the obstacle is small (indicated by the hatched area along the curve h_{2T} in Fig. 5), which is thus accompanied by a large downward excursion of the interface. This nearly singular behavior has additional implications for the thermal structure and variability near the obstacle, as discussed in section 5.

e. *Regime V (h_{1P}, $h_{2T} < h < 1$)*

In this regime, the lower layer is totally blocked and the upper layer is partially blocked. The interface relief, as plotted schematically in Fig. 6e, accentuates the downward displacement of the interface, which may become depressed everywhere. The throughflow in the upper layer is expelled to the left rim of the obstacle by a Taylor column anchored at the right edge of the obstacle.

f. *Regime VI ($1 < h$)*

In this regime, both layers are totally blocked, and the solution becomes a trivial one, with unperturbed level interface and a purely barotropic flow, as plotted in Fig. 6f. Again, the transition from Regimes V to VI is abrupt (the upper hatched area in Fig. 5), accompanied by a rebound of the depressed interface to its unperturbed level, which is in the opposite sense from that when the lower layer becomes totally blocked.

One recalls that in a homogeneous fluid, a seamount is more effective than an island in disturbing the flow in the far field through the generation of an anticyclonic circulation. The discussions here show additionally that in a stratified fluid, only a submerged seamount can perturb the interface and generate a baroclinic flow.

5. Discussion

Although only a two-layered fluid was considered, the interface reliefs deduced above can be combined to construct a thermal structure of a multiple-layered fluid. For example, if there is significant throughflow over the obstacle, one deduces a thermal structure as shown schematically in Fig. 8 when one faces downstream. There is doming of the density surfaces over the obstacle, the amplitude of which decreases toward the surface. The domes are displaced to the left if Taylor columns are formed and they are punctuated by level terraces over the right flank marking the overlapping region of the Taylor columns. For all density surfaces intersecting the obstacle wall, on the other hand, there is net downward displacement; that is, while the density surfaces may remain elevated to the left of the obstacle, they are more than compensated by a pronounced dipping along the right flank of the obstacle. In the case when the obstacle is so tall as to totally block the up-

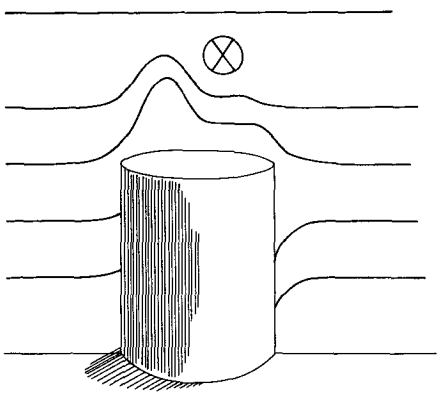

FIG. 8. A schematic for the thermal structure in a multiple-layer fluid when there is significant throughflow over the obstacle top (facing downstream).

Unauthenticated | Downloaded 01/15/25 03:25 PM UTC

stream flow, the density surfaces should be level and remain unperturbed by the obstacle.

These deductions compare favorably with observations over the Emperor Seamount Chain (Roden and Taft 1985), particularly over Suito and Kinmei Seamounts where deep measurements are available and where the upstream flows are better defined. The hydrographic section across the Suito Seamount (their Figs. 4 and 5) has exhibited mesoscale features (of the scale of the baroclinic deformation radius or a few tens of kilometers) as depicted in Fig. 8, including the bottom intensified doming of the density surfaces over the obstacle and the conspicuous dipping of the density surfaces at the west flank of the seamount, consistent with an upstream flow coming from the north (the Subarctic Current). Over the Kinmei Seamount (their Figs. 9 and 10), however, the density surfaces are relatively flat despite its greater height, consistent with the fact that Kinmei Seamount has extended nearly to the surface and may have totally blocked the upstream flow (the Kuroshio Extension).

One notes that the bulging of the layer at the level of the obstacle top simply reflects the sharpness of the transition from partial to total blocking. Since the far field is constantly perturbed in the ocean, one would then expect an amplified excursion of the density surfaces near the top edge of the obstacle, or an enhanced thermal variability there. Whether the apparent pumping of the layer that alternates between partial and total blocking would contribute significantly to the lateral exchange of fluid is a question of practical importance and merits further investigation.

As deduced in section 4c, if the stratification is sufficiently weak, or typically when the baroclinic deformation radius is smaller than half the obstacle radius, there may be ventilation of the Taylor column in the lower layer. This appears to be the case of the Maude Rise in the Weddell Sea where extensive hydrographic measurements are available (Gordon and Huber 1990). If one uses a density difference of $0.2\sigma_t$ across the thermocline, its unperturbed depth of 150 m, an ocean depth of 5 km, and a Coriolis parameter of 1.3×10^{-4} s^{-1}, one estimates the baroclinic deformation radius to be about 5 km, much smaller than the obstacle radius (about 150 km). So for all practical purposes, the fluid is homogeneous, and the Taylor columns in the two layers, if present, should be nearly aligned. If in addition, one uses $U \approx 10$ cm s^{-1}, the Rossby number is about 5×10^{-3}, or two orders of magnitude smaller than the nondimensionalized obstacle height (greater than 0.5). One thus expects extensive Taylor columns over the Maude Rise with the throughflow confined to the very fringe of the obstacle. Since there is intense cooling in the area, according to earlier discussions, one then expects a significantly weakened stratification and ventilation of even the lower layer over the Maude Rise, consistent with their observations.

As discussed by Gordon and Huber (1984) and Martinson (1990), among others, this deep convection can upwell heat from below to cause a polynya, an open area enclosed by ice which, however, may be transitory due to shallowness of the water above the Maude Rise and hence limited heat supply. But if a significant portion (i.e., the northern portion) of the Taylor column is sheared off by a surging upstream flow, it may then tap the deep reservoir of heat and result in a more sustained polynya in the Weddell Sea. This contrasting behavior of the polynya on and off the Maude Rise is consistent with observations (Streten 1973; Comiso and Gordon 1987). The shedding of the Taylor column may also partially explain the warm cells observed near the Maude Rise (Gordon and Huber 1984). The assessment of the above scenario of the Weddell polynya, as being seeded by a preconditioned Taylor column over the Maude Rise sheared off by a surging upstream flow, requires further theoretical and observational studies.

Acknowledgments. I want to thank F. Biolley for useful discussions, LuAnne Thompson for pointing out an overlooked result of Johnson (1978), and an anonymous reviewer for detecting a serious error in the frictional solution. I also want to thank many of my colleagues for commenting on the manuscript. This research is supported by the Office of Naval Research under Grant N-0001487-k0204 (DLE).

APPENDIX A

Streamlines Near a Stagnation Point

If one sets the streamfunction to zero at the stagnation point, its Taylor expansion about this point in the Cartesian coordinates x and y leads to

$$\psi \approx \psi_{xx}x^2 + 2\psi_{xy}xy + \psi_{yy}y^2, \qquad (A.1)$$

where the subscripts indicate partial derivatives. Setting (A.1) to zero, one then has the equation that governs the streamlines passing through the stagnation point. Letting $s \equiv y/x$ be the slope of such streamlines about the x axis, it then satisfies the equation

$$\psi_{yy}s^2 + 2\psi_{xy}s + \psi_{xx} = 0, \qquad (A.2)$$

which has at most two real roots, characterizing two intersecting streamlines. Letting q be the vorticity of the flow, one has an additional equation

$$\psi_{xx} + \psi_{yy} = q. \qquad (A.3)$$

For an irrotational flow ($q = 0$), one sees from (A.2) and (A.3) that there are indeed two streamlines intersecting at a right angle at the stagnation point. Accordingly, the stagnation point is isolated, and the flow may not vanish along any finite curve, a well-known property of the irrotational flow.

Unauthenticated | Downloaded 01/15/25 03:25 PM UTC

For a fluid with finite q, let us align the x axis with the tangent of one of the streamlines at the stagnation point, which implies through (A.2) $\psi_{xx} = 0$ and through (A.3) $\psi_{yy} = q$. The other root to (A.2) is then given by

$$s = 2\psi_{xy}/\psi_{yy} = -2\psi_{xy}/q. \quad \text{(A.4)}$$

If $\psi_{xy} = 0$, then $s = 0$. That is, there are no intersecting streamlines, and hence there may be a finite region of stagnation, in contrast to the irrotational case. Only at the point where $\psi_{xy} \neq 0$ are there intersecting streamlines, which however span an angle that deviates finitely from the right angle because of finite q.

APPENDIX B

The Solution for the Homogeneous Fluid in the Frictional Regime ($d \ll \alpha/\epsilon \ll 1$)

From the vorticity equation (3.3), one observes that the relative vorticity vanishes in both the outer and inner regions, or

$$\nabla^2\psi = 0 \quad \text{for} \quad r \neq 1. \quad \text{(B.1)}$$

To derive the matching conditions at $r = 1$, one first integrates the continuity equation (3.1) across the topographic jump to arrive at

$$[ud]_I^O = 0, \quad \text{(B.2)}$$

where I and O indicate the inner and outer variables. Under the constraint $d \ll 1$, (B.2) yields

$$u_O = -\frac{\partial\psi_O}{\partial\theta} = 0 \quad \text{at} \quad r = 1, \quad \text{(B.3)}$$

or the cylindrical boundary is a streamline for the outer flow. The other matching condition is derived by integrating (3.4) across the topographic jump to yield

$$[u + \alpha d^{-1}v]_I^O = 0, \quad \text{(B.4)}$$

or, using (B.3),

$$d^{-1}\frac{\partial\psi_I}{\partial\theta} + \alpha d^{-2}\frac{\partial\psi_I}{\partial r} = \alpha\frac{\partial\psi_O}{\partial r} \quad \text{at} \quad r = 1. \quad \text{(B.5)}$$

The solution to (B.1), (B.3), and (B.5) is

$$\psi_O = (r - r^{-1})\sin\theta, \quad \text{(B.6)}$$

$$\psi_I = 2d^2(1 + d^2\alpha^{-2})^{1/2} r \sin(\theta + \tan^{-1} d/\alpha). \quad \text{(B.7)}$$

APPENDIX C

The Solution for Regime I ($h < h_{2P}$)

The solution to (4.5) and (4.6) is

$$\eta = \begin{cases} r_C^{-1} h I_1(r_C^{-1}) K_0(r_C^{-1} r), & r > 1 \quad \text{(C.1)} \\ h[1 - r_C^{-1} K_1(r_C^{-1}) I_0(r_C^{-1} r)], & r < 1. \quad \text{(C.2)} \end{cases}$$

The barotropic flow ψ_T satisfying (4.10) is given by (Ingersoll 1969)

$$\psi_T = \begin{cases} r\sin\theta - \frac{1}{2}\epsilon^{-1} h \ln r, & r > 1, \quad \text{(C.3)} \\ r\sin\theta + \frac{1}{4}\epsilon^{-1} h(1 - r^2), & r < 1. \quad \text{(C.4)} \end{cases}$$

From (4.8) and (4.9), it is trivial to show that the stagnation point is first formed in the lower layer at the right edge of the obstacle when

$$h = h_{2P} = \epsilon\left[\frac{1}{2} + \gamma(1 - \gamma)^{-1} I_1(r_C^{-1}) K_1(r_C^{-1})\right]^{-1}. \quad \text{(C.5)}$$

APPENDIX D

The Solution for Regime IV ($R_C < r_C$, $h_{2T} < h < h_{1P}$)

In the outer region ($r > 1$), η is given by

$$\eta = b_0 K_0(r_C^{-1} r) + a_1 K_1(r_C^{-1} r)\sin\theta, \quad \text{(D.1)}$$

where

$$b_0 = -\frac{1}{2} r_C^{-1}(1 - \gamma)\hat{h} K_1^{-1}(r_C^{-1}),$$

$$a_1 = -(1 - \gamma) r_C^{-2} K_1^{-1}(r_C^{-1}) A,$$

$$A = \left[1 + \frac{1}{2} r_C^{-1}(1 - \gamma) K_0(r_C^{-1}) K_1^{-1}(r_C^{-1})\right]^{-1}.$$

The barotropic component as defined in (4.8) and (4.9) is given by

$$\psi_T = r\sin\theta + c\ln r + c_1 r^{-1}\sin\theta, \quad \text{(D.2)}$$

where

$$c = -\frac{1}{2}\gamma\epsilon^{-1}\hat{h},$$

$$c_1 = -(1 - \gamma)A\left[1 + \frac{1}{2} r_C^{-1} K_0(r_C^{-1}) K_1^{-1}(r_C^{-1})\right],$$

and the baroclinic component ψ_C is as given by (4.11). In the inner region ($r < 1$), the solution is

$$\psi_1 = \frac{1}{4}\epsilon^{-1}\hat{h}(1 - r^2) + \frac{1}{2}(1 - \gamma) r_C \epsilon^{-1} \times \hat{h} K_0(r_C^{-1}) K_1^{-1}(r_C^{-1}) + Ar\sin\theta. \quad \text{(D.3)}$$

To derive the blockage curve h_{2T}, one notes from (D.1) that η peaks at the left edge of the obstacle. By setting $\eta = \hat{h}$ at $r = 1$, $\theta = -\pi/2$, one derives the corresponding $\hat{h}$ as

$$\hat{h} \equiv \gamma[h_{2T} - (1 - \gamma)] = \epsilon(1 - \gamma) r_C^{-2} A^2. \quad \text{(D.4)}$$

Since from (D.3), the stagnation of the upper-layer flow first occurs at the right edge of the obstacle, to derive the blockage curve h_{1P}, one sets $\psi_{1r} = 0$ at $r = 1$, $\theta = \pi/2$ to derive the corresponding $\hat{h}$ as

Unauthenticated | Downloaded 01/15/25 03:25 PM UTC

$$\hat{h} \equiv \gamma[h_{1P} - (1 - \gamma)] = 2\epsilon A. \qquad (D.5)$$

To derive an equation for the critical stratification R_C, one sets $h_{1P} = h_{2T}$ to yield

$$\gamma = 1 - 2R_C[R_C^{-1} - K_0(R_C^{-1})K_1^{-1}(R_C^{-1})]^{-1}. \qquad (D.6)$$

REFERENCES

Batchelor, G. K., 1970: *An Introduction to Fluid Dynamics.* Cambridge University Press, 615 pp.

Comiso, J., and A. L. Gordon, 1987: Recurring polynya over the Cosmonaut Sea and the Maude Rise. *J. Geophys. Res.*, **92,** 2819–2833.

Csanady, G. T., 1982: *Circulation in the Coastal Ocean.* D. Riedel, 279 pp.

Gordon, A. L., and B. A. Huber, 1984: Thermohaline stratification below the southern ocean sea ice. *J. Geophys. Res.*, **89,** 641–648.

——, and ——, 1990: Southern Ocean winter mixed layer. *J. Geophys. Res.*, **95,** 11 655–11 672.

Gould, W. J., R. Hendry, and H. E. Huppert, 1981: An abyssal topographic experiment. *Deep-Sea Res.*, **28,** 409–440.

Hide, R., 1961: Origin of Jupiter's Great Red Spot. *Nature,* **190,** 895–896.

Hogg, N. G., 1973: On the stratified Taylor column. *J. Fluid Mech.*, **58,** 517–537.

Ingersoll, A. P., 1969: Inertial Taylor columns and Jupiter's Great Red Spot. *J. Atmos. Sci.*, **26,** 244–252.

Johnson, E. R., 1978: Trapped vortices in rotating flow. *J. Fluid Mech.*, **86,** 209–224.

Martinson, D. G., 1990: Evolution of the southern ocean winter mixed layer and sea ice; open ocean deepwater formation and ventilation. *J. Geophys. Res.*, **95,** 11 641–11 654.

Owens, W. B., and N. G. Hogg, 1980: Oceanic observations of stratified Taylor column near a bump. *Deep-Sea Res.*, **27,** 1029–1045.

Proudman, J., 1916: On the motion of solids in a liquid possessing vorticity. *Proc. R. Soc., London* **A92,** 408–424.

Roden, G. I., and B. A. Taft, 1985: Effect of the Emperor Seamounts on the mesoscale thermohaline structure during the summer of 1982. *J. Geophys. Res.*, **90,** 839–855.

Streten, N. A., 1973: Satellite observations of the summer decay of the Antarctic sea-ice. *Archiv. Meteor. Geophys. Bioklim.*, **A22,** 119–134.

Takematsu, M., and T. Kita, 1978: Vortex shedding from "Taylor Columns." *J. Phys. Soc. Japan,* **45**(5), 1781–1782.

Taylor, G. I., 1917: Motion of solids in fluids when the flow is not irrotational. *Proc. R. Soc. London,* **A93,** 99–113.

——, 1923: Experiments on the motion of solid bodies in rotating fluids. *Proc. R. Soc. London,* **A104,** 213–218.

Van Dyke, M., 1982: *An Album of Fluid Motion.* The Parabolic Press, 176 pp.

Unauthenticated | Downloaded 01/15/25 03:25 PM UTC